



Article

Experimental Analysis of a Novel Adaptively Counter-Rotating Wave Energy Converter for Powering Drifters

Guoheng Wu ¹, Zhongyue Lu ¹, Zirong Luo ^{1,*}, Jianzhong Shang ¹, Chongfei Sun ¹ and Yiming Zhu ²

¹ College of Intelligence Science and Technology, National University of Defense Technology, Changsha 410073, China; wuguoheng09@163.com (G.W.); strideryue@163.com (Z.L.); jz_shang_nudt@163.com (J.S.); sunchongfei@yeah.net (C.S.)

² School of Mechanical, Aerospace and Civil Engineering, University of Manchester, Manchester M17JR, UK; yiming.zhu@manchester.ac.uk

* Correspondence: luozirong@nudt.edu.cn; Tel.: +86-731-8457-4932

Received: 12 March 2019; Accepted: 9 May 2019; Published: 1 June 2019



Abstract: Nowadays, drifters are used for a wide range of applications for researching and exploring the sea. However, the power constraint makes it difficult for their sampling intervals to be smaller, meaning that drifters cannot transmit more accurate measurement data to satellites. Furthermore, due to the power constraint, a modern Surface Velocity Program (SVP) drifter lives an average of 400 days before ceasing transmission. To overcome the power constraint of SVP drifters, this article proposes an adaptively counter-rotating wave energy converter (ACWEC) to supply power for drifters. The ACWEC has the advantages of convenient modular integration, simple conversion process, and minimal affection by the crucial sea environment. This article details the design concept and working principle, and the interaction between the wave energy converter (WEC) and wave is presented based on plane wave theory. To verify the feasibility of the WEC, the research team carried out a series of experiments in a wave tank with regular and irregular waves. Through experiments, it was found that the power and efficiency of the ACWEC are greatly influenced by parameters such as wave height and wave frequency. The maximum output power of the small scale WEC in a wave tank is 6.36 W, which allows drifters to detect ocean data more frequently and continuously.

Keywords: wave energy absorption; drifters; experiments; sustainable power system; performance characteristics

1. Introduction

The sea is the general term for the continuous saltwater body that covers the Earth's surface. The ocean covers about 70.8% of the earth's surface, accounting for 97.2% of the earth's water, and is rich in minerals [1], marine product resources, and energies [2]. As scientists deepen their research on the ocean, accurate observations of the marine environment are increasingly important, especially the ocean currents. Satellite-tracked surface drifting buoy (drifters) observe currents, sea surface temperature, atmospheric pressure, winds, and salinity [3]. Figure 1 shows the main components of the SVP drifter. At present, there are two basic sizes of SVP drifters: the original, relatively large SVP drifter and the new "mini" version (Figure 2) [4]. They have a thermistor (metallic thermometer) on their base, and an underwater drogue, or sea anchor, located 15 m below the ocean surface, connected to the buoy by a long, thin tether, as shown in Figure 2. After years of development, a total of 1417 drifters were deployed in the National Oceanic and Atmospheric Administration's (NOAA, U.S. Department of Commerce) contribution to the Global Drifter Program (GDP) [4].

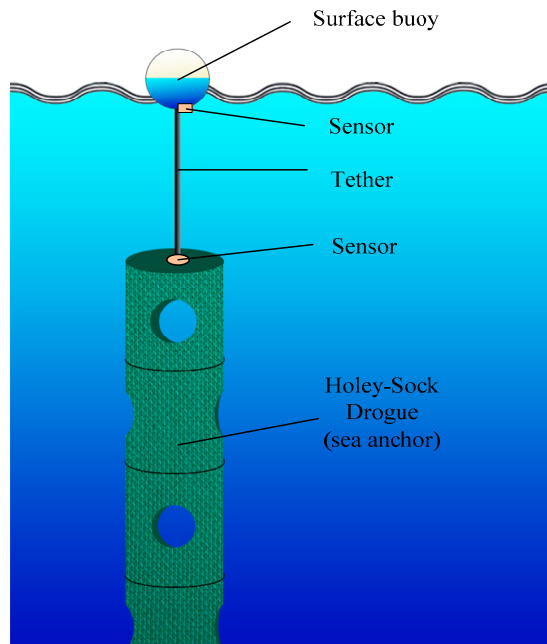


Figure 1. Structure of a drifter [4].

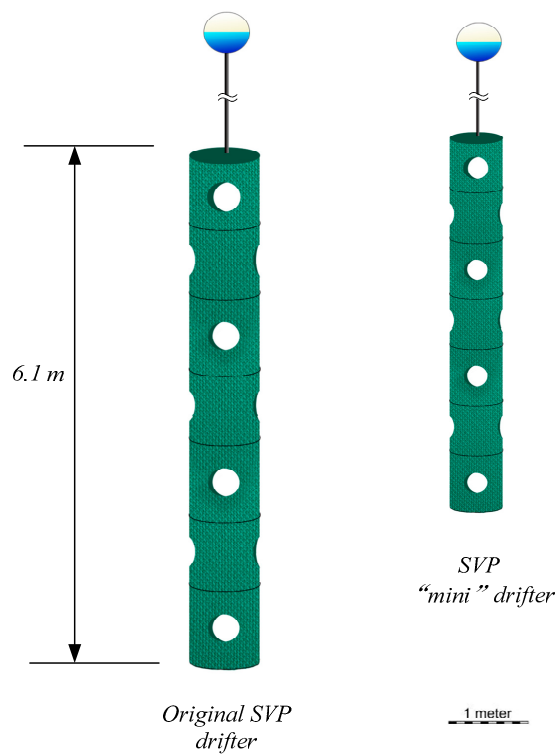


Figure 2. Schematic of two basic sizes of Surface Velocity Program (SVP) drifters [4].

The modern drifter is a relatively lean instrument—44 pounds with 16 foot drogues—costing around \$1700 each [5]. The GDP drifters are fitted with diode-protected, alkaline D-Cell, 12 V, 56 Ah battery packs. Once deployed, a modern SVP drifter lives an average of 400 days before ceasing transmission. To ensure the drifters’ life time is long enough, the sampling frequency of the drifters cannot be too high, and the drifters are inactive during most of the time at sea, because the battery capacity is limited. SVP drifters are typically sampled at intervals of about 5 min.

Researchers in various countries are trying to overcome the power constraint of floaters. Floaters demand high-density energy sources and lithium is light with high oxidation energy. PolyPlus Battery Company has developed a prototype lithium-seawater battery that is attractive for powering long-duration autonomous oceanographic vehicles (floats and underwater gliders) [6]. Using thermal energy is also a way to supply power for floaters. Several articles [7–9] have studied the feasibility of supplying power to floaters with thermal power. An energy storage system has been demonstrated on an Argo style float and has been implemented in a thermal version of the Slocum glider. The energy harvesting system is based on a phase change material with a freeze–thaw cycle that pressurizes hydraulic oil, which is converted to electrical energy [10]. Another option is solar energy [11,12]. A 65 cm² solar array was used to power an Argos beacon in reference [13]. However, the primary lithium batteries are hazardous to the ocean's environment, the temperature difference between cooler deep and warmer shallow or surface seawaters in many waters is not big enough to generate electricity, and floating buoys on drifters are too small and spherical, so it is difficult to use solar energy for power generation.

The drifters' work area is full of waves, so the research team hopes to design a wave power plant for drifters without affecting the way the drifters work, which will increase their service life. If there is enough power, drifters can also make measurements more frequently and the amount of data each drifter can measure will increase, so it can provide more accurate data for the study of ocean circulation. In addition, by rational design, increasing the drag of the underwater system makes drifters less affected by the sea wind force.

Wave energy, with the advantages of high energy density and wide distribution, is an inexhaustible renewable clean energy source, and considered an ideal energy source for the power supply of the drifters. For more than two centuries, inventors have proposed many different devices to utilize wave power for human purposes [14–16], and several research papers relating to ocean wave energy conversion have been emerged in an endless stream [17–20]. Control strategies for wave energy conversion systems also have been studied in several papers [21–24]. António F. de O. Falcão [25] categorized ocean wave energy converters (WECs) into three main categories: oscillating water column, overtopping device, and point absorber. The oscillating water column (OWC) [26,27] is by far the most developed and investigated wave energy device [28]. Dorrell et al. [29] described the OWC operation, modeling, and experimental equipment in 2004. The overtopping device works much like a hydroelectric dam, which is another type of ocean WEC. The Wave Dragon, placed in Nissum Bredning, Denmark, was grid-connected in May 2003 as the world's first offshore WEC [30]. Reference [31] presents results on the wave loading acting on a hybrid WEC named Overtopping BReakwater for Energy Conversion (OBREC). A point absorber is an offshore floating device which captures energy from its wave induced motion via hydraulic rams and a high-pressure power take-off (PTO) system [32]. The Archimedes wave swing (AWS), mainly consisting of a bottom-fixed air-filled cylindrical chamber (the silo) and a movable upper cylinder (the floater), is an offshore fully-submerged WEC. Several articles [33–35] have discussed modeling and control of an AWS-based wave energy conversion system. Another type of ocean WEC is produced by Ocean Power Delivery Ltd. (Scotland, UK), named Pelamis [36], which consists of floaters moving along with respect to each other when waves pass. The point absorber (PA) is a heaving buoy type wave energy converter. The analysis and discussion of PA-based wave energy devices have been discussed in several articles [37–39]. However, the current wave energy research is mainly for commercialization, and mostly focuses on the power grid. The WECs are not necessary to be designed and installed in the deep seas. Only a small amount of literature has studied the energy supply of small monitoring buoys [40]. Since the power needs of drifters are relatively small and most of them work in deep seas, it is difficult to directly apply the existing wave energy technology to drifters.

The surface float of an SVP drifter ranges from 30.5 cm (the smallest mini) to 40 cm in diameter. The WEC, which provides energy supplementation for drifters, first needs to meet three requirements: (1) The WEC needs to be a small power generation device—because drifters are relatively small in size and limited in space, large energy conversion devices are not suitable for this role. In addition, the

energy requirement of the drifter device only needs to meet the demand of its detection functions, so there is no need to install a large energy conversion device; (2) The point absorber is better suited for power supplying to the drifter, since the size of drifters is relatively small compared to the wavelength of random waves in the sea, and the size of the point absorber is relatively the smallest in terms of the wavelength of the incident wave [41,42]; (3) The WEC does not affect the function of SVP drifters.

Referring to the distribution of the global drifter array and sea state wave characteristics and average global distribution [43], the distribution of SVP drifters and the sea state at their location can be known. The sea state at most drifters' locations is greater than 2, so when the wave energy device can generate a certain amount of electricity under a low sea state to meet the needs of the drifter, the wave energy device can solve the problem of the drifter's battery life.

Considering the working environment and energy demands of drifters, this paper proposes a counter-rotating self-adaptable wave energy converter (WEC) for powering drifters. The wave energy-powered SVP drifter concept is illustrated in Figure 3 for a counter-rotating self-adaptable PTO module fixed under the drogue. The WEC uses an underwater absorber to convert the reciprocating motion in the vertical direction into the relative rotation of the two blade groups of the absorber, to drive the generator to generate electricity. The buoy is a sphere with a radius of 25 cm. The size of the absorber is shown in the figure. The drogue can ensure the drifter follows the movements of the water and is unaffected by wind and instruments, and reduce slippage between the drifter package and the water [4], the drifter is mainly used to investigate ocean currents and other parameters like temperature or salinity. Common electrical devices include the radio frequency transmitter, atmospheric pressure sensor, temperature sensor, and salinity sensor. Therefore, the WEC placed at a depth of about 30 m from the ocean surface will hardly affect the measurement results of sensors near the wave surface.

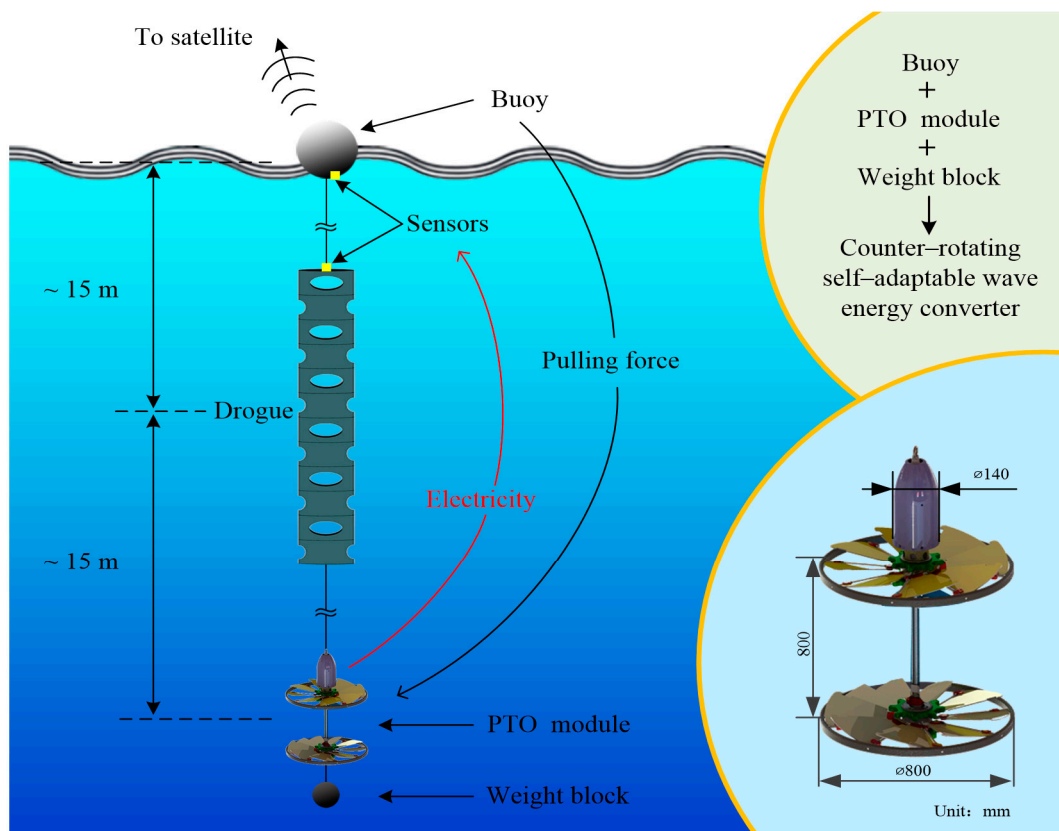


Figure 3. Wave energy-powered SVP drifter concept with a counter-rotating self-adaptable WEC.

The WEC is a point absorber with the advantages of easy installation on SVP drifters and a simple power generation process. Through this simple and effective integration, it will provide continuous

power supply to SVP drifters and will hardly affect the monitoring results. It is expected to be an efficient way for improving the sampling intervals of drifters, on the basis of an easy integration method.

The counter-rotating self-adaptable WEC has been numerically simulated in [44], where computational fluid dynamics (CFD) technology was used to numerically analyze the simplified model of the WEC. Based on the computer simulation of the interaction between seawater and the WEC, the effects of water velocity and blade inclination on the power and efficiency characteristics of the device have been investigated. Figure 4 shows the main work and research results and conclusions of [44]. The absorbed power of the upper absorber increases with the increase in relative water flow velocity. The ideal blade inclination is 20–30° when the velocity through the blades is low (≤ 1.4 m/s), and 30–40° when the velocity is high (≥ 2.0 m/s). However, there is obviously a large boundary effect in the bucket in the experiment in [44]. It is very necessary to verify the principle and characteristics of the WEC in the artificial wave basin. In addition, there are many factors affecting the performance of the counter-rotating self-adaptable WEC. Wave conditions, absorber weight, and other factors will have an impact on the final power generation. The dynamic simulation of the whole system is time-consuming and laborious, and it is difficult to ensure the accuracy of the calculation. Therefore, it is necessary to verify and further study the new WEC in the wave basin.

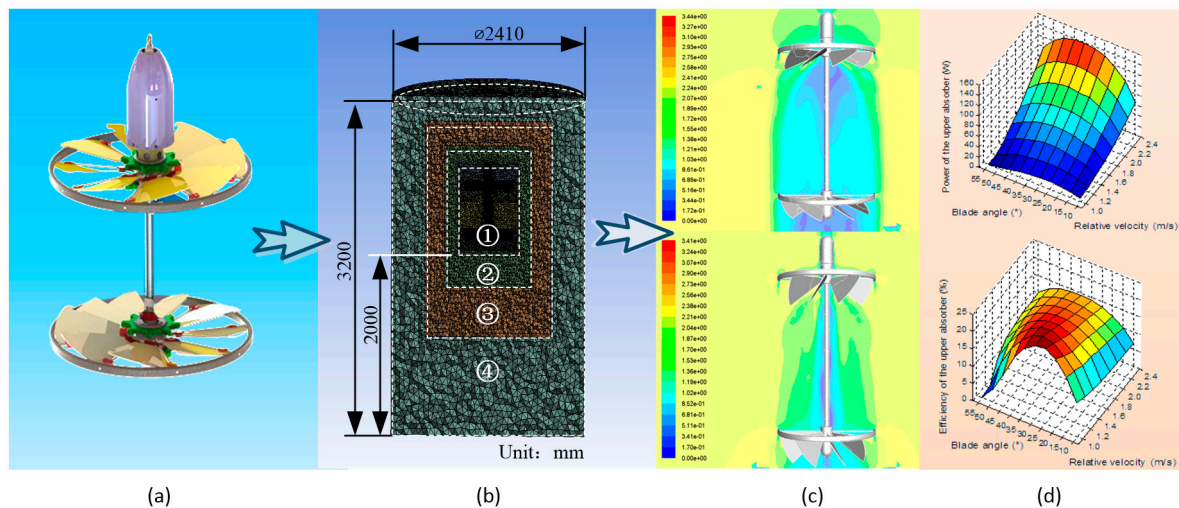


Figure 4. Design concept and mechanical structure: (a) simplified numerical model; (b) vertical section of the mesh model; (c) velocity contours of the vertical section of the absorber with different blade angles; (d) combined effect of blade angle and relative velocity on the performance of the upper absorber.

In this paper, the experimental analysis method was used to analyze the most important factors (wave height and wave period) affecting the power generation efficiency of the WEC. This paper is organized as follows: Section 2 describes the conversion principle of the WEC, Section 3 presents the experimental arrangement and different experimental conditions, Section 4 discusses the power generation performance of the ACWEC, Section 5 draws the conclusions.

2. Design Concept

2.1. Basic Mechanism

Table 1 shows the P-M spectrum characteristics of several sea states. According to current scientific understanding of ocean, the waves on the surface of the sea are usually very strong. However, for sea state 3, when the depth reaches 15 m or over, the fluctuation of water will become extremely small. According to the research results of Basom [45], the amplitude of fluctuation is about halved at a depth of 1/9 the wavelength; while the depth reaches twice the wavelength, the movement of the water tends to move in the direction of the flow with little or no oscillation.

Table 1. Pierson–Moskowitz sea spectrum.

Sea State	Significant Wave Height (m)	Average Length of Waves (m)	Significant Range of Periods (s)	Average Period (s)
1	0–0.1	4	1–4	1.5
2	0.1–0.5	9	1.5–6	3
3	0.5–1.25	17	2–7.5	4
4	1.25–2.5	27.5	2.5–9.5	5
5	2.5–4	39	3–11	6.5
6	4–6	68	4–15.5	8
7	6–9	130	5.5–22	11

According to Basom [45], as the depth of water increases, the radius of the orbital circle decreases rapidly, as shown in Figure 5a. A = at deep water. The elliptical motion of fluid particles decreases rapidly with increasing depth below the surface. B = at shallow water (ocean floor is now at B). The elliptical movement of a fluid particle flattens with decreasing depth [45]

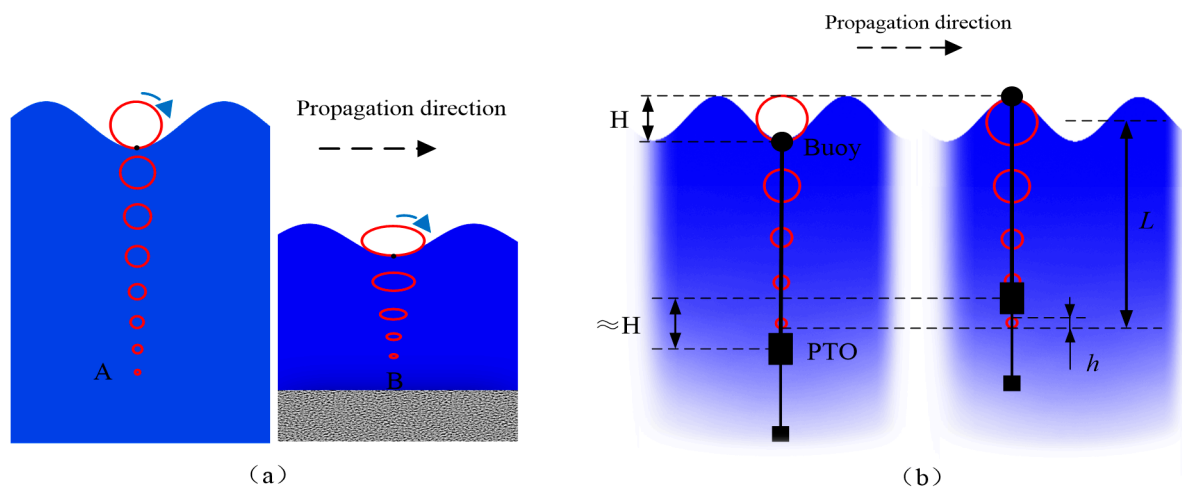


Figure 5. Motion of a particle and WEC in an ocean wave: (a) the movement of water particles in deep water and shallow water; (b) the SVP drifter in ideal deep-water.

The point absorber typically uses a steel cable to secure one end to the sea floor or to a stationary platform, which are considered the reference coordinates of the system. When the ocean waves drive the buoy to move relative to the reference coordinates, the wave energy in the waves is captured and converted into mechanical energy. Similarly, the root cause of the counter-rotating self-adaptable WEC is the interaction between water particles and the absorber blades. Only when there is relative motion between the water particles and the blades can the blades obtain torque under the push of water particles.

As shown in Figure 5b, assuming that the wave is an ideal deep-water wave, the displacement of the wave surface particle in the vertical direction is H , and the displacement of the water particle at the depth L is h in the vertical direction. The displacement of the PTO in the vertical direction driven by the buoy is about H , and the displacement of the PTO relative to the surrounding water particles is $\Delta = H - h$. Thus, water particles passing through the PTO can push the PTO blades to generate torque. In the case where the wave height H and the period are constant, when the water depth L is larger, h is smaller, and Δ is larger, the more the water particles passing through the PTO, the more the absorber absorbs the wave energy.

The buoy is affected by the horizontal component of the wave force and will deviate from the origin position in the horizontal direction. Assuming that the horizontal position of the PTO is unchanged, as shown in Figure 6, there is an angle θ between the tether and the vertical direction:

$$\theta = \arcsin \frac{r}{l}, \tag{1}$$

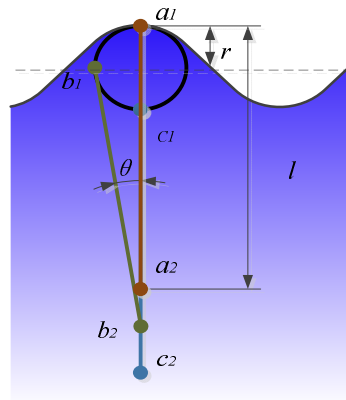


Figure 6. The effect of wave motion on the position of PTO.

Therefore, increasing the length of the tether can mitigate the effect of the horizontal component of the wave motion on the WEC. The wave height range in sea state 3 is 0.5–1.25 m, and the depth of the PTO is 30 m, then the maximum angle is θ_{max} .

$$\theta_{max} = \arcsin \frac{1.25/2}{30} = 1.2^\circ, \tag{2}$$

It can be seen that the horizontal component of the wave motion has little effect on the PTO. In addition, the lateral cross-sectional area of the drogue is large, and the lateral damping is large in the seawater. Therefore, it is difficult for the wave to change the horizontal position of the PTO through the buoy and cable. The moving direction of the PTO can be approximated as vertical. The assumption about the horizontal position of the PTO is reasonable.

The absorber captured wave energy mainly through a group of eight blades. Each blade could swing freely around its own axis over a range of angles. As shown in Figure 7a, the α was the free swing angle range of one of the blades, which was about $\pm 1.2^\circ$. The angular direction of the blade was always the same as the direction in which the water flow impacted the blade group. The directions of the upper blade group and lower blade group were clockwise and counterclockwise, respectively, as shown in Figure 7b. When the water flowed through the absorber, the two groups of blades were respectively driven to rotate clockwise and counterclockwise, and their difference in rotational speed was the input speed of the generator. The detailed structural design is introduced in the next section.

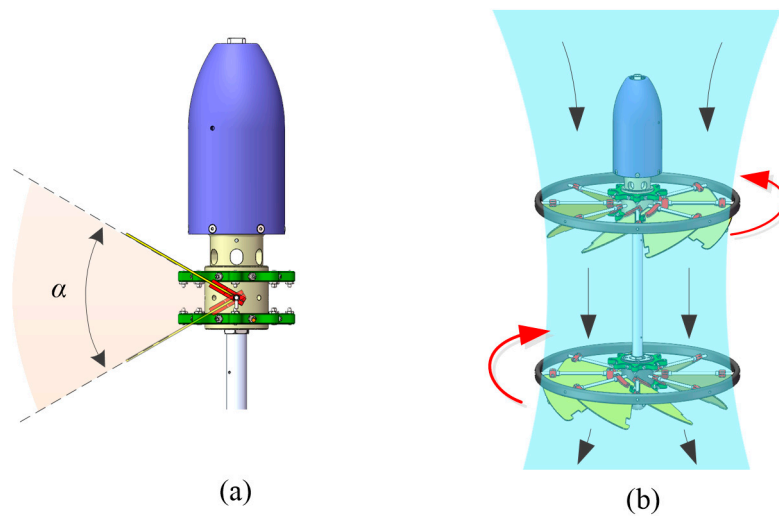


Figure 7. Basic function and form of the blade: (a) free swing angle range of one of the blades; (b) the directions of the upper blade group and lower blade group rotate in opposite directions.

2.2. Mechanical Design

Considering these realistic situations, the wave energy supply strategy of the drifter was designed as shown in Figure 8a. The energy supply model contained three parts: the buoy, power cable, and power take-off (PTO). In the following analysis, the drogue is no longer separately analyzed and can be considered a part of the PTO. The buoy itself can be considered the floating body of the system, which was used to absorb the kinetic energy of the sea waves. Meanwhile, it could collect and detect data on the surface of the sea as a working drifter. The PTO was connected to the buoy through a power cable, which acted not only as a connection but also an energy and control signals transmission channel between the buoy and WEC.

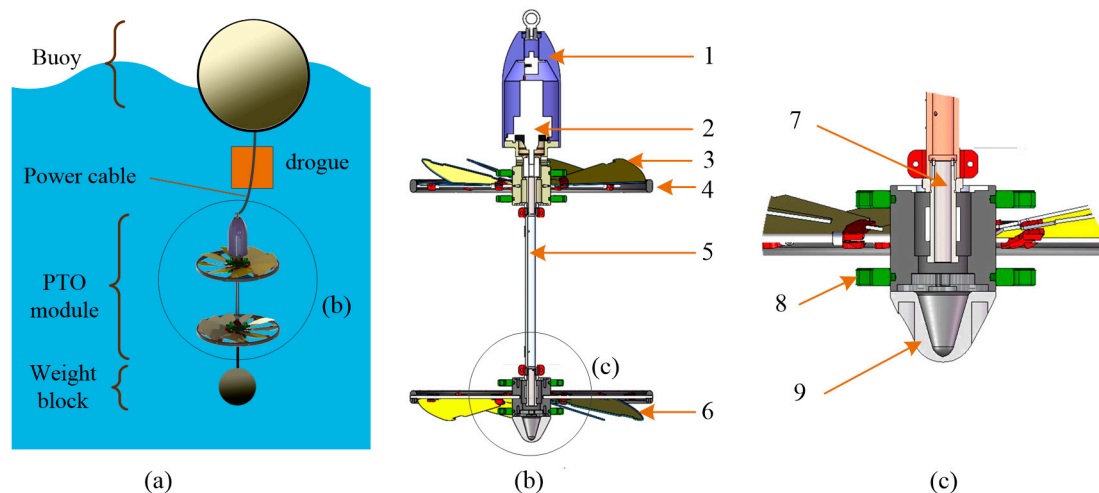


Figure 8. Design concept and mechanical structure: (a) schematic diagram of the design concept; (b) section view of the mechanical structure (1. water shield; 2. direct current (DC) generator; 3. upper blade group (UBG); 4. caging device; 5. supporting tube; 6. lower blade group (LBG)); (c) partial section view of mechanical structure (7. transmission shaft; 8. adjustable ring for blade angle; 9. water shield).

The advantages of this design can be displayed in four aspects: (1) The PTO is small and convenient for the drifter to carry; (2) Being designed as a point absorber is beneficial for using the buoy of the drifter as a floating body to absorb wave energy; (3) In the working process, only the buoy works on

the surface of the sea, while the PTO works in the hydrostatic water deep in the sea. The WEC does not affect the monitoring of the SVP drifter; (4) It is easy for this PTO to integrate into existing drifters.

As shown in Figure 8b,c, the main working parts of the PTO included the upper blade group (UBG) (3), lower blade group (LBG) (6), and direct current (DC) generator (2). Each blade group consisted of eight fan-shaped blades with caging devices. Each fan-shaped blade could swing up and down freely. The rotating shafts of the DC generator and LBG were connected through a transmission shaft (7) and a shaft coupling. The external frames of the DC generator and UBG were also connected through another shaft coupling. To ensure the structural rigidity, a supporting tube (5) was installed outside the transmission shaft. A caging device (4) was used to maintain the circumferential position of the blades in the upper and lower blade groups. The angle of each blade in the UBG and LBG was regulated by two adjustable rings (8) above and below each blade group. Water shields (1, 9) were installed on the PTO for water proofing.

2.3. Working Principle

The buoy moved up and down under the action of wave force and it drove the underwater PTO to move in a heaving motion through the power cable. The whole working process was divided into two processes, as shown in Figure 9.

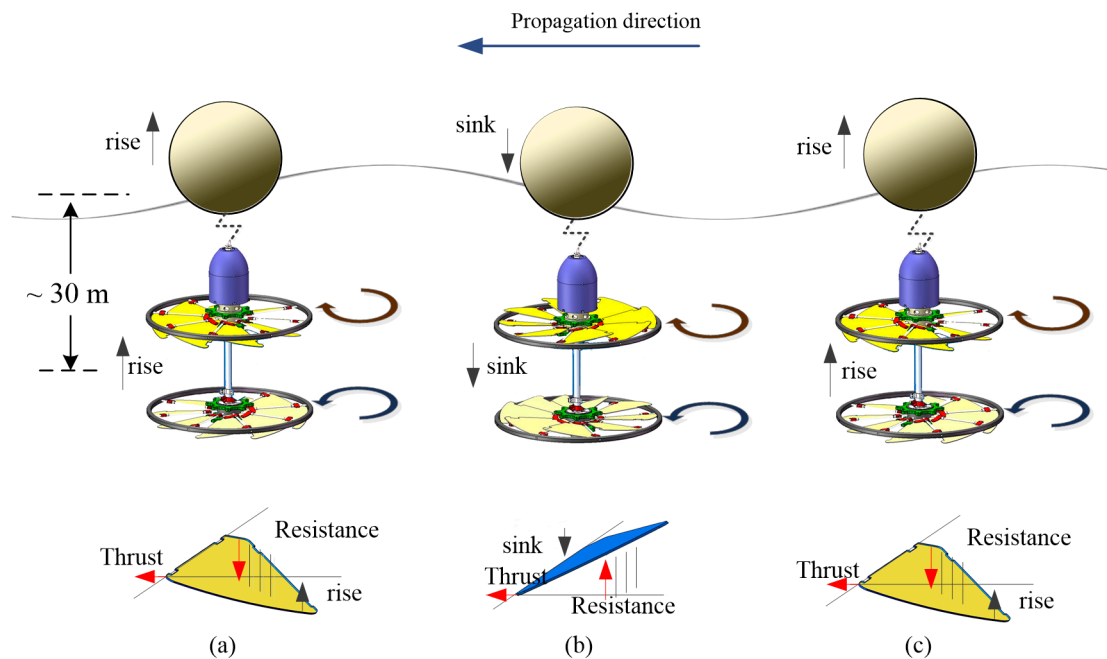


Figure 9. Working principle: (a,c) rising process; (b) sinking process.

Process 1 was the process of the buoy being pushed by the wave from the trough to the crest. The underwater PTO was dragged by the power cable to rise with the surface buoy. All blades were adaptively swung down to the maximum deflection angle under the influence of water flow, as shown in Figure 9a. Due to the limitation of the adjustable ring, the blades remained in the inclined state after reaching the maximum angle of inclination. The water body continued to impact the inclined blades and produced thrust to push the blades forward. Since the blades were circumferentially arranged, the UBG rotated clockwise. Likewise, the lower blade group (LBG) rotated counterclockwise.

Process 2 was the process of the whole device descending from the crest to the trough under its own gravity. If the buoy sank, the underwater PTO also sank because of the gravity force. All blades were adaptively swung up to the maximum deflection angle under the influence of water flow, as shown in Figure 9b. The water body continued to impact the inclined blades and produce thrust to

push the blades forward. The UBG continued to rotate clockwise without changing direction. Likewise, the LBG continued rotating counterclockwise.

When the whole device hit another crest, as shown in Figure 9c, process 1 was repeated. When the surface buoy came to a balanced position (the maximum of the crest and the minimum of the trough), the blades were in the swinging process and unable to provide thrust. Therefore, the UBG and LBG maintained their clockwise and counterclockwise rotation direction, respectively, because of inertia.

Based on the above analysis, the conclusion can be drawn that, no matter whether it is in the rising process or sinking process, the PTO can passively adjust the angle of the blades to ensure the upper and lower blade groups are rotating clockwise and counterclockwise respectively, thus ensuring the PTO's stability in the absorption process. Meanwhile, the double-layered blade groups can automatically balance the overall torque of the underwater PTO. This WEC had three main steps to absorb wave energy: (1) the buoy absorbed the kinetic energy of the waves and transformed it into the kinetic energy of the PTO's heaving motion; (2) the kinetic energy of the PTO transformed into the rotating mechanical energy of the UBG and LBG; and (3) the UBG and LBG drove the generator to generate electricity.

This adaptively counter-rotating WEC is innovative in the following ways: (1) The WEC can adapt to different sea states. The adjustable blade angle of the UBG and LBG can be adjusted by presetting or adjusting online, so that the WEC can achieve the optimal working state under sea waves of different amplitudes and frequencies. No matter how the wave height changes, the upper blade group (UBG) rotates clockwise and the lower blade group (LBG) rotates counterclockwise, both of which will not be affected by fluctuating amplitude in the process of interaction between the PTO and the water body; (2) The energy conversion process is simple. Wave energy can be directly absorbed through the rotating blade groups and then converted into electricity without intermediate conversion components, such as pneumatic turbines or hydraulic equipment.

3. Experiment Platform

3.1. Prototype and Method

In order to verify the power generation performance of the WEC, a semi-scale ACWEC was designed and manufactured, as shown in Figure 8. Referring to the Pierson–Moskowitz spectrum (PM spectrum), when the sea state is 3, the wave height in the real ocean is 0.5–1.25 m. The maximum wave height that can be generated in the wave tank is 0.6 m, so it cannot generate the wave height in full scale in a small tank. In order to enable the wave tank to simulate the corresponding wave height of sea state 3, the geometry of the buoy and the absorber was reduced by 50%. According to the similarity principle of fluid, the wave height generated by the wave tank can be approximated as a proportional reduction of sea state 3 wave height.

The outer caging rings of the UBG and LBG were made of aluminum alloy—eight fan-shaped blades per blade group. Due to its high modulus and strength and its good corrosion resistance, a carbon fiber tube was used for the blade shaft. The rest of the PTO was mainly made of stainless steel 304. A DC generator with built-in accelerator was integrated into the PTO. The maximum output power was 30 W. The mass of the PTO was 6 kg.

The experimental platform in the wave tank was set up as shown in Figure 10. The platform contained a wave tank, a DAQ card (Data Acquisition Card), a control room, two wave height measuring sensors (Sensor (A) and Sensor (B)), and an upper computer with data acquisition program. In order to verify the design concept of the ACWEC, which was introduced in Section 2, there was a flexible connection (tether) between the buoy and the PTO.

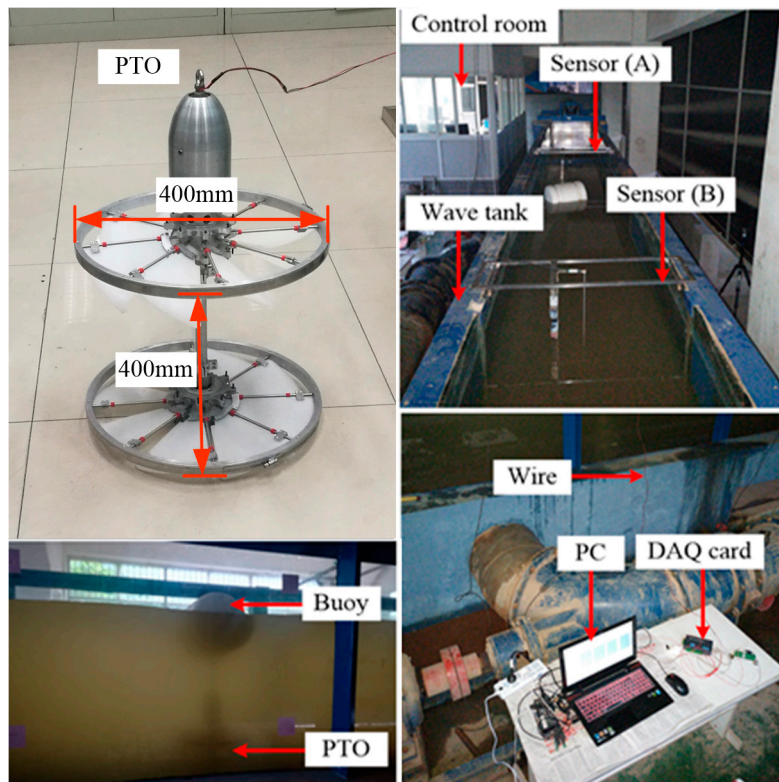


Figure 10. Experimental platform in a wave tank.

A servo motor-driven irregular wave-making machine was installed at the head of the tank. A board that pushed water into waves and the mechanical frame of the wave-making machine were installed about 1.5 m from the head of the water tank. There was an energy dissipation net at the back of the wave-making machine to prevent splashing, and another energy dissipation net at the other end of the wave tank to eliminate waves. The wave-making system consisted of hardware equipment and control software. The hardware equipment mainly consisted of a board that pushed water into waves, mechanical frame, lower computer, servo motor and driver, servo controller, position sensor, motion control interface card, wave height measuring sensors, computer, and the acquisition system. The control software mainly included various wave-making control programs, wave spectrum analysis, and wave feature statistical analysis procedures.

The control room could control the wave period, wave height, and waveform of the waves in the wave tank. The experimental platform used a data acquisition card (DAQNavi-USB4716) to collect data. Due to the limitations of the DAQ card measurement range, voltage signals could only be measured in the range of $(0 \pm 10V)$.

As shown in Figure 11, the total length of the wave tank was $L_1 = 22.5$ m, the height of the wave tank was $H_a = 1$ m, and the width of the wave tank was 0.8 m. The floating buoy was a cylinder with a diameter of 0.3 m and a height of 0.35 m, the material of the buoy was foam plastic. In order to make the wave tank have a full waveform with a maximum wave height of 0.3 m, the water depth in the wave tank was set to $H = 0.6$ m. As shown in Figure 8, the height of the PTO was 0.4 m. Considering the depth of the wave tank was not sufficient to accommodate the ACWEC's complete device (buoy and PTO), this test designed a water basin in the tank at a distance $L_3 = 6$ m from the head of the tank. The length of the water basin was $L_2 = 2$ m. The width of the water basin was equal to the width of other locations in the wave tank, which was 0.8 m. The height of the water basin was $H_b = 0.8$ m. Sensor (A) and Sensor (B), with a measuring range of 0–0.6 m, were used to measure the wave height before and after the ACWEC, respectively. The distance between Sensor (A) and Sensor (B) was 3 m, with the ACWEC located at the midpoint of the two sensors. In the experiment, the ACWEC was laid

out as shown in Figure 11. The buoy was connected to the PTO with a rope. At the bottom of the ACWEC (below the PTO), a cylinder drogue with a mass of M_1 was connected to adjust the weight of the ACWEC.

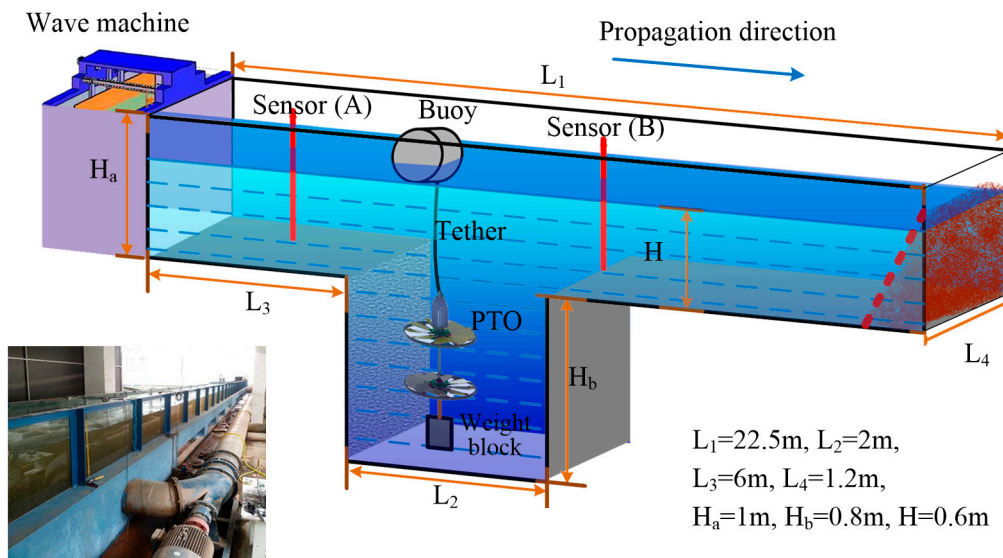


Figure 11. Experimental schematic.

Since the water depth of the wave tank was only 0.6 m, when the wave height was greater than 0.3 m the wave was broken, so the maximum wave height was 0.3 m in the experiment. On the other hand, it was found in the experiment that when the wave height created by the wave tank was less than 0.15 m, the power generated by the ACWEC was very weak, even equal to zero, so the minimum wave height in this paper was 0.15 m. Therefore, the wave height range in the experiment described in this paper was 0.15–0.3 m.

The typical wave spectrum in the ocean of sea state 3 is 0.14–1.0 Hz. However, in the experiment, when the wave period of the created wave was less than 1.5 s, a complete waveform could not be produced when the wave height was high (greater than 0.25 m). When the wave period of the created wave was greater than 3 s, the output power of the ACWEC was seriously reduced and the power generation efficiency was not improved either. Thus, the wave period range in this experiment was 1.5–3.0 s. By the frequency limitations of the wave tank, the spectrum 0.33–0.66 Hz was selected in the experiments.

In the experiments, the main source of error was measurement error, which consisted of the wave height error of Sensor (A) and Sensor (B) and the voltage error of the DAQ. The measurement error of Sensor (A) and Sensor (B) was $\pm 5\%$ of the measured value. After the analog input of the DAQ was calibrated, the measurement error of the DAQ was ± 0.1 V. Since the data measured in the experiment was much larger than the error range and only the power generation feasibility of the ACWEC is analyzed in this paper, very accurate measurement values were not required. Therefore, the influence of the error on the power generation performance was not considered in the discussions.

3.2. Power and Efficiency Calculation Method

In a sea state, the average energy density per unit area of gravity waves on the water surface is proportional to the wave height squared, according to linear wave theory: [46,47]

$$E = \frac{1}{16} \rho g H^2, \quad (3)$$

where E is the mean wave energy density per unit of horizontal area (J/m^2)—the sum of kinetic and potential energy density per unit of horizontal area. The potential energy density is equal to the kinetic energy [44,45], both contributing half to the wave energy density E , as can be expected from the equipartition theory. H is the wave height, ρ is the density of water, and g is the gravity.

As the waves propagate, their energy is transported. The energy transport velocity is the group velocity. As a result, through a vertical plane of unit width perpendicular to the wave propagation direction, the wave energy flux is equal to:

$$P_0 = E \cdot c_g, \tag{4}$$

where c_g is the group velocity (m/s). Due to the dispersion relation for water waves under the action of gravity, the group velocity depends on the wavelength λ , or equivalently on the wave period T . Furthermore, the dispersion relation is a function of the water depth h . As a result, the group velocity behaves differently in the limits of deep or shallow water and at intermediate depths.

Waves in the limits of shallow water, with wavelengths λ much larger than the water depth h , travel with the following phase velocity [48]:

$$c_g = \sqrt{gh}, \tag{5}$$

where g is the acceleration by gravity and c_g the phase speed. Since this shallow water phase speed is independent of the wavelength, shallow water waves do not have frequency dispersion. Therefore, the wave energy flux with a wave height of H , through a vertical plane of unit width perpendicular to the wave propagation direction, is equal to:

$$P_0 = \frac{1}{16} \rho g H^2 \sqrt{gh}, \tag{6}$$

$$P_{input} = P_1 - P_2 = \frac{1}{16} \rho g \sqrt{gh} (H_1^2 - H_2^2), \tag{7}$$

where H_1 is the wave height before the WEC, H_2 is the wave height after the WEC, and P_{input} is the input power to the WEC.

The direct current generator includes a conductive disk or cylinder that rotates in a plane that is perpendicular to a uniform static magnetic field. A potential difference is created between the center of the disc and the rim. The polarity of the electricity depends on the direction of rotation and the orientation of the field. The power of the generator is the output power of the WEC:

$$P_{output} = \frac{U^2}{R}, \tag{8}$$

where U is the voltage at both ends of the external resistance and R is the value of the external resistance.

This paper studies the overall efficiency (η) of the PTO. The overall efficiency (η) is defined as the conversion efficiency from the kinetic energy captured by the buoy to the generated power in the form of electricity:

$$\eta = \frac{P_{output}}{P_{input}} = \frac{16U^2}{\rho g R \sqrt{gh} (H_1^2 - H_2^2)}, \tag{9}$$

3.3. The Effect of System Mass on Power and Efficiency

Inertial-based kinetic energy harvesters are modelled as second-order, spring-mass systems. The generic model of kinetic energy harvesters was first developed by Williams and Yates [49]. Figure 12 shows a generic model of such a generator, which consists of a seismic mass, m , and a spring with the spring constant of k .

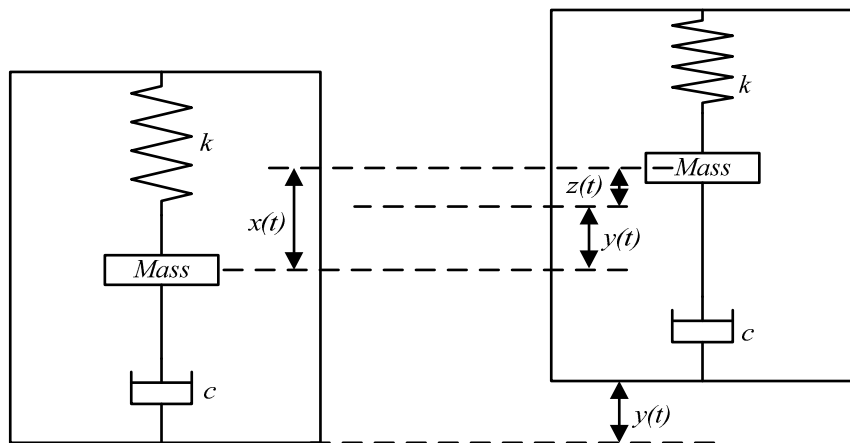


Figure 12. Generic model of kinetic energy harvesters.

When the WEC vibrates, the mass moves out of phase with the WEC housing. There is a relative movement between the mass and the housing. This displacement is sinusoidal in amplitude and can drive a suitable transducer to generate electrical energy. c is the damping coefficient, which consists of mechanically induced damping (parasitic damping) coefficient c_m and electrically induced damping coefficient c_e , i.e., $c = c_m + c_e$. $y(t)$ is the displacement of the generator housing and $z(t)$ is the relative motion of the mass with respect to the housing. For a sinusoidal excitation, $y(t)$ can be written as $y(t) = Y\sin(\omega t)$, where Y is the amplitude of the vibration and ω is the angular frequency of vibration.

For the analysis, it is assumed that the mass of the vibration source is much greater than the seismic mass in the generator, and the vibration source is unaffected by the movement of the generator. Then, the differential equation of the movement of the mass with respect to the generator housing from the dynamic forces on the mass can be derived as follows:

$$m \frac{d^2 z(t)}{dt^2} + c \frac{dz(t)}{dt} + kz(t) = -m \frac{d^2 y(t)}{dt^2}. \tag{10}$$

As mentioned above, damping in kinetic energy harvesters consists of mechanically induced damping (parasitic damping) and electrically induced damping. The overall damping factor of the system, ξ_T , is given by

$$\xi_T = \frac{c}{2m\omega_r} = \frac{c_m + c_e}{2m\omega_r} = \xi_m + \xi_e, \tag{11}$$

where $\xi_m = c_m/2m\omega_r$ is the mechanically induced damping factor and $\xi_e = c_e/2m\omega_r$ is the electrically induced damping factor. $\omega_r = \sqrt{k/m}$ is the resonant frequency.

Assume that the input is a sinusoid excitation, i.e., $y(t) = \sin(\omega t)$. The solution to Equation (10) is given by:

$$z(t) = \frac{m\omega^2 Y}{k - m\omega^2 + j\omega c} \sin(\omega t), \tag{12}$$

Or

$$z(t) = \frac{\omega^2}{\sqrt{(\omega_r^2 - \omega^2)^2 + \left(\frac{c\omega}{m}\right)^2}} Y \sin(\omega t + \varphi), \tag{13}$$

$$\varphi = \tan^{-1}\left(\frac{c\omega}{k - \omega^2 m}\right), \tag{14}$$

The average power dissipated within the damper—the sum of the power extracted by the transduction mechanism and the power lost in mechanical damping—is given by:

$$P = c \left(\frac{dz(t)}{dt} \right)^2, \tag{15}$$

Equations (13) and (15) give the average power dissipated within the damper as follows:

$$P(\omega) = \frac{m\xi_T Y^2 \left(\frac{\omega}{\omega_r} \right)^3 \omega^3}{\left[1 - \left(\frac{\omega}{\omega_r} \right)^2 \right]^2 + \left(2\xi_T \frac{\omega}{\omega_r} \right)^2}, \tag{16}$$

When the generator is at resonance, i.e., $\omega = \omega_r$, the power dissipation reaches maximum. The maximum dissipated power is

$$P = \frac{mY^2 \omega_r^2}{4\xi_T} = \frac{mY^2 \omega_r^2}{4(\xi_m + \xi_e)}, \tag{17}$$

The power dissipation is the sum of the maximum electrical energy extracted by the transduction mechanism, P_e , and mechanical loss, P_m . P_e and P_m are as follows:

$$P_e = \frac{\xi_e m Y^2 \omega_r^2}{4(\xi_m + \xi_e)}, \tag{18}$$

$$P_m = \frac{\xi_m m Y^2 \omega_r^2}{4(\xi_m + \xi_e)}, \tag{19}$$

Maximum power conversion from the mechanical domain to the electrical domain occurs when $\xi_m = \xi_e$, i.e., damping arising from the electrical domain equals mechanical losses. Therefore, the maximum electrical power that can be extracted by the kinetic energy harvester, P_e , is given by

$$P_e = \frac{P}{2} = \frac{mY^2 \omega_r^2}{8\xi_m} = \frac{Y^2 k^{\frac{3}{2}} \sqrt{m}}{4c_m}, \tag{20}$$

It can be seen that not only does the increase in wave height increase the output power of a power generation system, but the increase in mass also improves the output power of the power generation system.

4. Results and Discussion

4.1. Generation Performance when the M_1 is 14.21 kg

The original design SVP drifters weigh 45 kg each. Mini drifters weigh 20 kg each [4]. In order to get close to the actual weight of the mini SVP drifters, experiments were conducted under 4.21 kg (the mass of the PTO is 6 kg, the sum mass of PTO and M_1 is 20.21 kg).

According to the above analysis, the wave height range described in this paper is 0.15–0.3 m. By the frequency limitations of the wave tank, the spectrum is 0.33–0.66 Hz. Figure 13 shows the wave curves when the wave height is 0.3 m and the wave period is 3 s. S1 is the wave curve after the ACWEC, which is measured by Sensor (B); S2 is the wave curve before the ACWEC, which is measured by Sensor (A). It can be seen that the wave height before the ACWEC is about 3 mm larger than the wave height after the ACWEC, meaning that the kinetic energy of the waves decreased when passing through the ACWEC. The gravity, friction, and the electricity generation process of the ACWEC consumed the decreased energy.

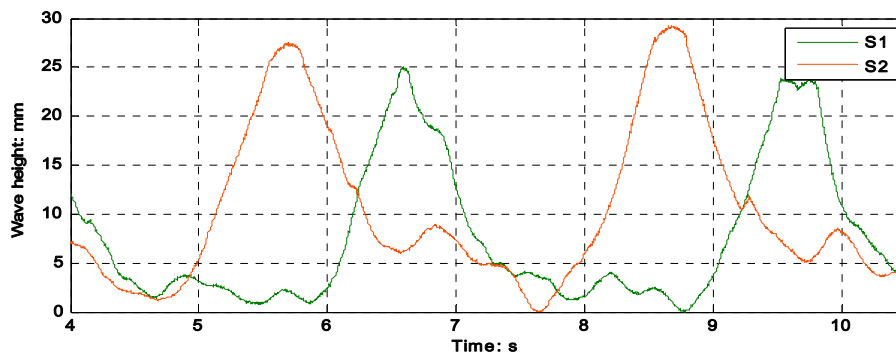


Figure 13. Waveform curves when the wave height is 0.3 m and the wave period is 3 s. (S1 is the wave curve after the ACWEC; S2 is the wave curve before the ACWEC).

Figure 14 shows the output voltage under different wave heights when the wave period of the created wave is 2 s. As shown in Figure 14, the larger the wave height, the larger the output voltage. The maximum output voltage of the PTO is at its maximum relative speed (the midpoint of the wave motion). The maximum output voltage is about 3.8 V. When the wave height is 0.15 m, the output voltage is very low. Based on the analysis in Section 2, it can be concluded that during the working process, when the rising movement and the sinking movement of the ACWEC is switching to each other, the adjustment of the blades (the blades swinging upward or downward to the next working position) on the UBG and LBG requires the consumption of a movement distance. When the wave height is 0.15 m, the working distance of the PTO is too short to meet the requirement for adjusting the blades, so the output voltage is very low.

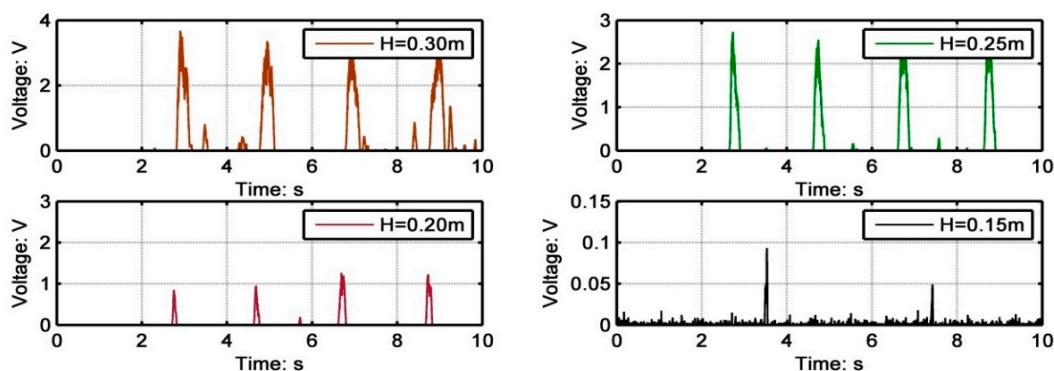


Figure 14. Voltage curves when the wave period is 2 s.

The power generation performance characteristics with different wave heights are shown in Figure 15. When the wave height of the created wave increases, the output power increases, and so does the power generation efficiency. As shown in Figure 15a, when the wave period was 2.5 s (0.4 Hz) and the wave height was 0.3 m, the maximum output power was 3.20 W. When the wave height was 0.15 m, the output power was relatively low, because the adjustment of the blades under the impact of the water needs to consume a certain distance. When the wave height was too little, the working distance of the PTO was too short to meet the requirements for adjusting the blades, which led to the blades not being able to work for a long time in the effective working place, resulting in the output power being the lowest. A similar phenomenon can be seen in Figure 14—the generator could not work sometimes and the output voltage was 0 V. As shown in Figure 15b, the output efficiency was lowest when the wave height was 0.15 m. Based on the comprehensive analysis above, when the wave height is relatively small, the generation process is less efficient, caused by two reasons: (1) The intermediate swinging process of the blades; (2) When the wave height decreases, the relative velocity between the PTO and water also decreases, which reduces the power generation efficiency. When the

wave period was 2 s (0.5 Hz) and the wave height was 0.3 m, the ACWEC was the most efficient, with an efficiency of 11.18%.

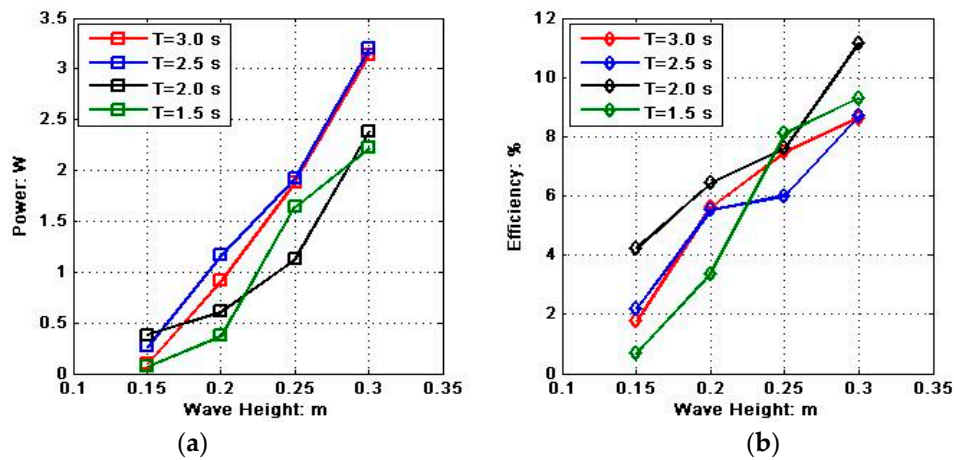


Figure 15. Generation performance of the ACWEC with different wave heights, $M_1 = 14.21$ kg: (a) power curve; (b) efficiency curve.

The power generation performance characteristics with different wave periods are shown in Figure 16. As shown in Figure 16a, when the wave period was 2.5 s (0.4 Hz), the generated power was higher than the power under other wave periods. No matter how the wave period value changes, an increase in wave height will increase the generated power and the generation efficiency. As shown in Figure 16b, the system obtains maximum power and maximum generation efficiency when the wave height is 0.3 m, under any wave period value. The generated power and power generation efficiency are always the lowest when the wave height is 0.15 m, sometimes even close to zero.

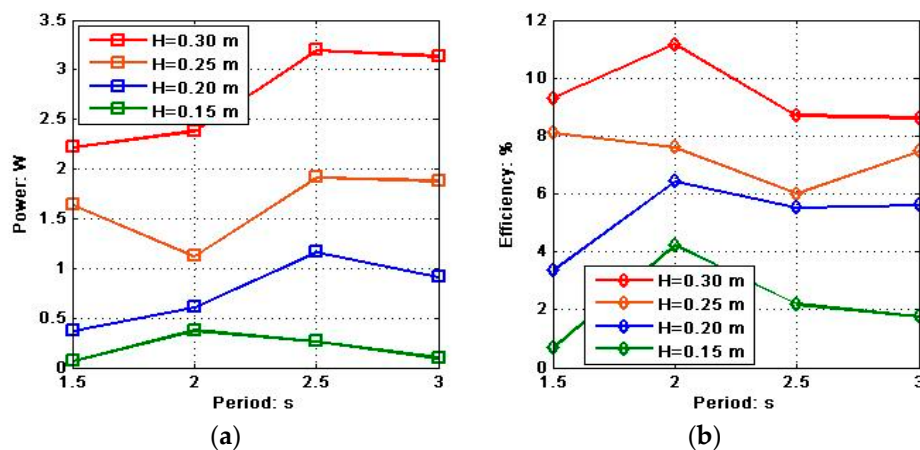


Figure 16. Generation performance of the ACWEC with different wave periods, $M_1 = 14.21$ kg: (a) power curve; (b) efficiency curve.

4.2. Generation Performance when the M_1 Is 20.11 kg

In order to observe the impact of increased mass of M_1 on the power generation performance, experiments were also conducted under $M_1 = 20.11$ kg (the sum mass is 26.11 kg).

The power generation performance characteristics with different wave heights and wave periods with $M_1 = 20.11$ kg are shown in Figures 17 and 18. As shown in Figure 17, the output power and generation efficiency increase with the increase in the wave height of the created waves. When the wave period was 2.5 s (0.4 Hz) and the wave height was 0.3 m, the maximum output power was

6.36 W. When the wave period was 2 s (0.5 Hz) and the wave height was 0.3 m, the ACWEC is the most efficient, with an efficiency of 11.87%.

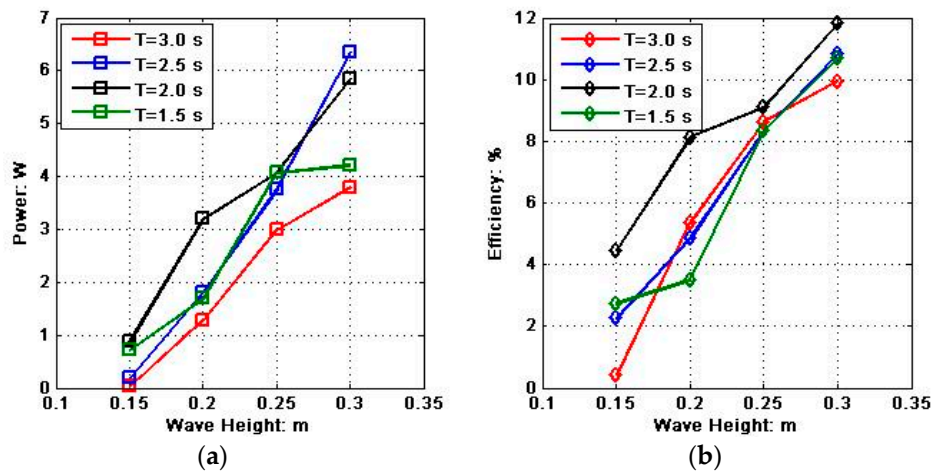


Figure 17. Generation performance of the ACWEC with different wave heights, $M_1 = 20.11$ kg: (a) power curve; (b) efficiency curve.

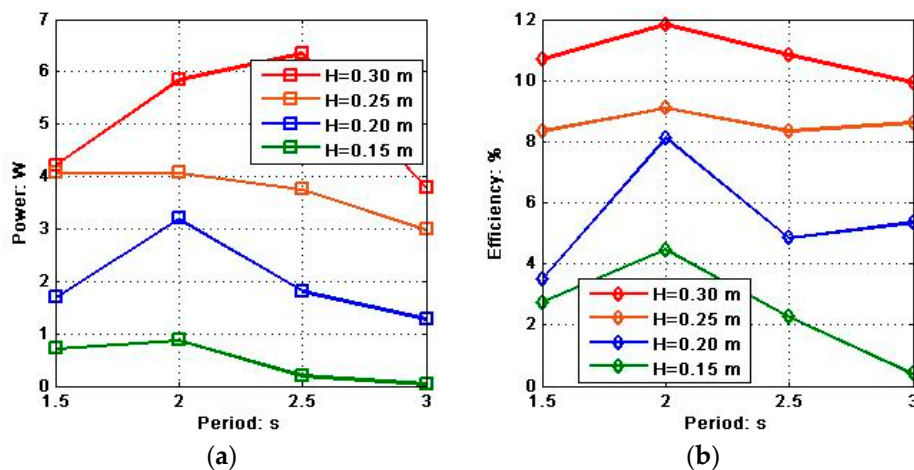


Figure 18. Generation performance of the ACWEC with different wave periods, $M_1 = 20.11$ kg: (a) power curve; (b) efficiency curve.

The power generation performance characteristics of the ACWEC with different wave periods under $M_1 = 20.11$ kg are shown in Figure 18. The system obtains maximum power and maximum generation efficiency when the wave height is 0.3 m, under any wave period value. As analyzed above, the generated power and power generation efficiency are always the lowest when the wave height is 0.15 m.

As shown in Figure 19, the generated power and power generation efficiency under $M_1 = 20.11$ kg have increased relative to the data under $M_1 = 14.21$ kg. The maximum generated power under $M_1 = 20.11$ kg is 3.16 W higher than the maximum generated power under $M_1 = 14.21$ kg. The power generation efficiency also increased by 0.69%.

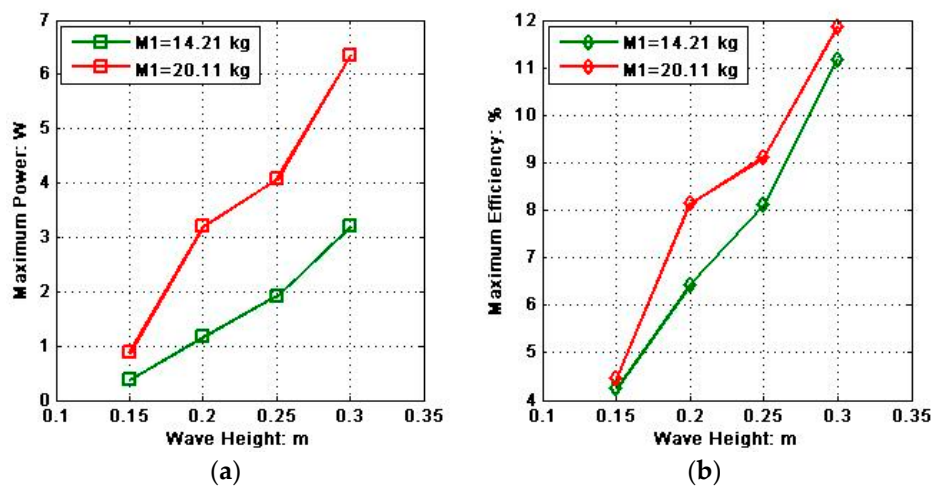


Figure 19. Comparison of generation performance of the ACWEC with different masses of M_1 : (a) the maximum power curve; (b) the maximum efficiency curve.

4.3. Generation Performance when the M_1 is 20.11 kg in Irregular Waves

Actual waves are random and extremely irregular, affected by wind speed and geographical conditions. This random phenomenon means that the characteristic values of waves at a particular point in time cannot be obtained. However, through a large number of observations and statistics, the seemingly irregular random waves actually have a certain degree of regularity, especially manifested in some characteristic parameters of the waves. Taking wave height and wavelength as examples, although the variation in wave height and wavelength is random, the number of occurrences of wave height and wavelength with a certain size is roughly certain. Figure 20 shows the curves of the waves measured at two points in the experiment as a function of time. Obviously, the waves have no regularity. However, waves can be analyzed with significant wave height and average wave period. The wave heights in the wave trains are arranged in descending order. The average of the largest 1/3 wave heights is called the significant wave height.

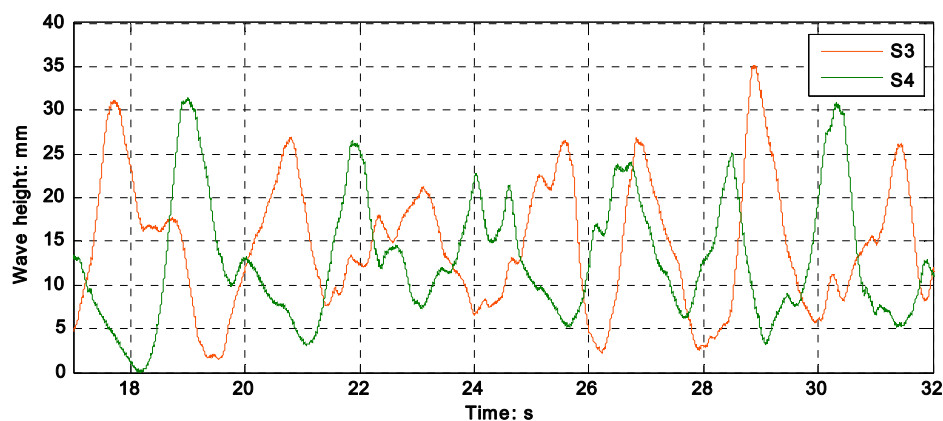


Figure 20. Wave curves when the significant wave height is 0.3 m and the average wave period is 3 s. (S3 is the wave curve before the ACWEC; S4 is the wave curve after the ACWEC.).

The theoretical calculation of the wave spectrum is complex. For this reason, marine researchers have obtained several calculation formulas for the wave spectrum, based on a large number of marine observations and theoretical analysis [50]. For example, the PM (Pierson–Moskowitz) spectrum, JONSWAP (Joint North Sea Wave Project) spectrum, SCOTT spectrum, and Wallops spectrum.

The PM spectrum is one of the simplest models used to describe a fully developed sea state. It is formulated in terms of the two parameters of significant wave height (H_s) and average wave period (T_z). It is the power spectral density of the sea state.

The PM spectrum is an empirical relationship, and it was arrived at by using wave measurements made in the North Atlantic by weather ships in the 1960s. It is applicable only to fully developed seas, i.e., the wind generating the waves has to blow for a very long time over a very large area/fetch. A modified form of the PM spectrum is recommended by the ITTC (international towing tank conference) [51].

$$S_{PM}(\omega) = \frac{\alpha g^2}{\omega^2} \exp\left[-\beta\left(\frac{g}{\omega U_{19.4}}\right)^4\right], \tag{21}$$

where $\alpha = 0.0081$ and $\beta = 0.7$ are numerical constants, g is gravity, and $U_{19.4}$ is the wind speed at 19.4 m above the sea surface.

In the experiment, a simplified spectral equation was used according to the Chinese national standard and the parameters of the wave tank:

$$S(f) = \frac{0.0005}{f^2} \exp\left[-\frac{0.001998}{f^4 H_s^2}\right], \tag{22}$$

where H_s is the significant wave height.

In the experiment, the significant wave height range was 0.15–0.3 m. By the frequency limitations of wave tank, the spectrum was 0.33–0.66 Hz. Figure 20 shows the wave curves when the significant wave height is 0.3 m and the average wave period is 3 s. S3 is the wave curve before the ACWEC, which was measured by Sensor (A); S4 is the wave curve after the ACWEC, which was measured by Sensor (B). It can be seen that the wave heights before the ACWEC were higher than the wave heights after the ACWEC. As analyzed in Section 4.1, the loss of wave energy is consumed by gravity, friction, and some of it is converted into electricity.

The power generation performance characteristics of the ACWEC with different significant wave heights under $M_1 = 20.11$ kg in irregular waves are shown in Figure 21. When the significant wave height of the irregular wave increases, the output power increases, and so does the power generation efficiency. As shown in Figure 21a, when the average wave period is 1.5 s (0.67 Hz) and the significant wave height is 0.3 m, the maximum output power is 3.71 W. When the significant wave height is 0.15 m, the output power is the lowest. As shown in Figure 21b, the output efficiency is also the lowest when the significant wave height is 0.15 m. When the average wave period is 2 s (0.5 Hz) and the significant wave height is 0.3 m, the ACWEC is the most efficient, with an efficiency of 10.77%. The power generation performance characteristics of the ACWEC with different average wave periods under $M_1 = 20.11$ kg in irregular waves are shown in Figure 22. The system obtains maximum power and maximum generation efficiency when the significant wave height is 0.3 m, under any average wave period.

Based on the above comprehensive experiments, the maximum output power is 6.36 W and the maximum generation efficiency is 11.87%. From Sections 2 and 3, it can be concluded that the working depth of the PTO is designed at 30 m. Due to the limitations of the wave tank, the working depth in these experiments was only about 0.8 m. The motion of the wave particle at that working depth is still a circle—in other words, the PTO at that depth still has a horizontal speed, which reduces power generation efficiency. Experiments in deeper wave tanks can improve power generation performance.

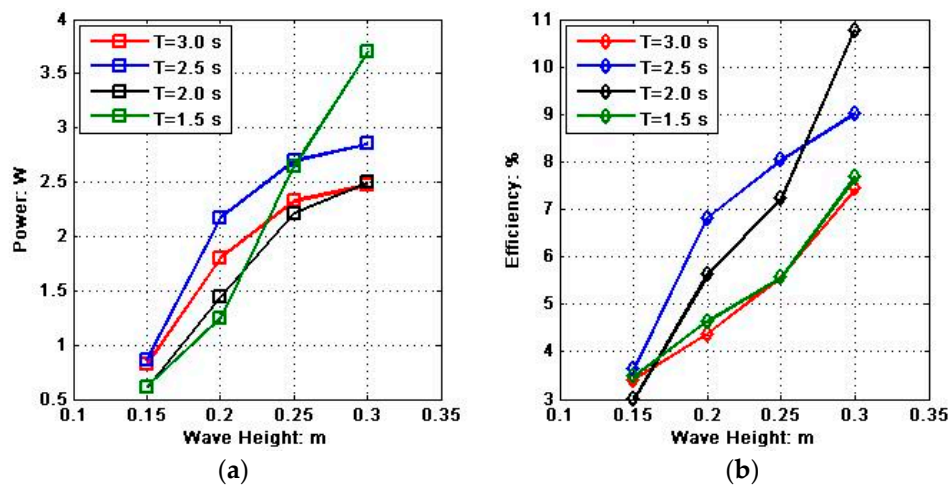


Figure 21. Generation performance of the ACWEC with different significant wave heights, $M_1 = 20.11$ kg: (a) power curve; (b) efficiency curve.

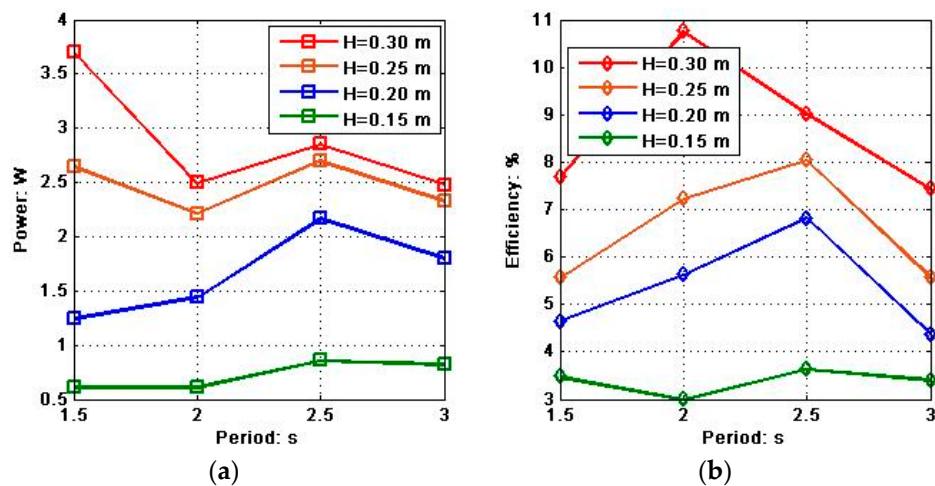


Figure 22. Generation performance of the ACWEC with different average wave periods, $M_1 = 20.11$ kg: (a) power curve; (b) efficiency curve.

5. Conclusions

This paper proposed an adaptively counter-rotating wave energy converter for powering drifters. In this paper, the power generation performances of the WEC in regular and irregular waves were studied, and the conclusions are drawn as follows:

- (1) The mechanism of the adaptively counter-rotating converter is feasible. The generated electricity is a direct current, and it can prove that the PTO can adaptively adjust the deflecting direction of the blades under the water impact direction so as to keep the unidirectional rotation of the UBG and LBG. Otherwise, the output current will be AC (Alternating Current). The underwater PTO can avoid damage from wind and waves on the surface of the sea. This WEC can theoretically adaptable to any sea state.
- (2) The interaction between the WEC and the water was analysed. The working depth of the PTO is equal to the length of the tether in current SVP drifters, which is 15 m. Due to the limitations of the wave tank, experiments under different conditions at a depth of 0.6 m were carried out. As a result, the maximum output power was 6.36 W and the maximum generation efficiency was 11.87%, with a wave height of 0.3 m. Experiments in deeper wave tanks will reduce the impact of horizontal flow velocity, which can improve power generation efficiency.

- (3) Experiments under $M_1 = 14.21$ kg and $M_1 = 20.11$ kg were carried out. Increasing the mass of M_1 will reduce the natural period of the ACWEC, which can improve the power generation performance of the ACWEC.
- (4) Experiments in irregular waves were also carried out. As a result, the maximum output power was 3.71 W and the maximum generation efficiency was 10.77% when the significant wave height is 0.3 m.

In conclusion, the parameters of the created waves were selected for analysis, which could effectively optimize the design of ACWECs and guide WECs to achieve optimal working status in different wave statuses and meet different energy requirements.

The GDP drifters are fitted with diode-protected, alkaline D-Cell, 12 V, 56 Ah battery packs to be able to work for around 400 days [52]. Due to the limitation of buoy volume, the battery capacity is not very large. This is also because the power demands of drifters are not very high. A power system with a maximum output power of 6.36 W is enough to make a drifter work continuously. This is an efficient way to improve the sampling intervals of drifters. The use of clean wave energy can reduce the amount of battery used and reduce the pollution of damaged batteries in seawater.

Although this paper has conducted a series of experiments in regular and irregular waves on the influence factors of the created waves, the research on WECs is still not thorough. Some important influencing factors, such as the blade angles, the number of blades, the distance between the UBG and LBG, and the stability of the output power, still need to be studied further.

Due to the limitation of the size of the wave tank, the waves generated in the wave tank are different from ocean waves. For example, deep water waves cannot be generated in the wave tank, and the water depth of the wave tank limits the position of the absorber such that it can only be placed close to the water surface. The semi-scale WEC experiment in the wave tank makes it difficult to simulate the case of an ACWEC in a real ocean. Experimental conclusions are based on the specific wave conditions in the wave tank. The wave tank experiment can only qualitatively verify the feasibility of the ACWEC and the influence of key parameters on the power generation performance of the ACWEC. In order to obtain more detailed and rigorous experimental results, an experiment of a full-scale ACWEC in the ocean needs to be carried out after completing a larger experimental prototype and obtaining better experimental support.

In addition, the entire marine environment is very complicated, and considering various failure modes of marine engineering structure, such as corrosion, bio-fouling and dynamic sediments, a new prototype of ACWECs with sufficient reliability needs to be designed. Finally, due to the high conductivity of seawater, an effective waterproofing method would increase the service life of the equipment.

Author Contributions: Conceptualization, Z.L. (Zirong Luo) and G.W.; methodology, Z.L. (Zhongyue Lu); software, C.S.; validation, G.W., Z.L. (Zhongyue Lu) and C.S.; formal analysis, J.S.; investigation, Y.Z.; resources, J.S.; data curation, Z.L. (Zhongyue Lu); writing—original draft preparation, G.W. and Z.L. (Zhongyue Lu); writing—review and editing, G.W.; supervision, J.S.; project administration, Z.L. (Zirong Luo); funding acquisition, Z.L. (Zirong Luo)

Funding: This research was funded by the Natural Science Foundation of China, grant number 51475465. The APC was funded by Zirong Luo.

Acknowledgments: The wave tank was provided by School of Hydraulic Engineering, Changsha University of Science and Technology, Changsha 410073, China.

Conflicts of Interest: The authors declare no conflict of interest.

References

- Petersen, S.; Krätschell, A.; Augustin, N.; Jamieson, J.; Hein, J.; Hannington, M. News from the seabed—Geological characteristics and resource potential of deep-sea mineral resources. *Mar. Policy* **2016**, *70*, 175–187. [[CrossRef](#)]
- Boud, R. *Status and Research and Development Priorities, Wave and Marine Accessed Energy*; DTI Report # FES-R-132, AEAT Report # AEAT/ENV/1054; UK Department of Trade and Industry (DTI): London, UK, 2003.
- The Global Drifter Program. Available online: <http://www.aoml.noaa.gov/phod/dac/index.php> (accessed on 11 June 2018).
- PhOD—The Global Drifter Program—What’s a Drifter? Available online: http://www.aoml.noaa.gov/phod/dac/gdp_drifter.php (accessed on 21 June 2018).
- Doing Their Part: Drifter Buoys Provide Ground Truth for Climate Data. Available online: <https://www.climate.gov/news-features/climate-tech/doing-their-part-drifter-buoys-provide-ground-truth-climate-data> (accessed on 12 June 2018).
- Davis, R.E.; Sherman, J.T. Evaluating a Lithium-Seawater Battery on Gliders. *J. Atmos. Ocean. Technol.* **2017**, *34*, 1175–1182. [[CrossRef](#)]
- Schofield, O.; Kohut, J.; Aragon, D.; Creed, L.; Graver, J.; Haldeman, C.; Kerfoo, J.; Roarty, H.; Jones, C.; Webb, D.; et al. Slocum gliders: Robust and ready. *J. Field Robot. Spec. Issue Spec. Issue Underw. Robot.* **2007**, *24*, 473–485. [[CrossRef](#)]
- Webb, D.C. Autonomous Propulsion within a Volume of Fluid. U.S. Patent No. 5,291,847, 8 March 1994.
- Jones, J.A.; Chao, Y.; Valdez, T.I. Phase Change Material Thermal Power Generator. U.S. Patent No. 7,987,674, 2 August 2011.
- Haldeman, C.; Schofield, O.; Webb, D.C.; Valdez, T.I.; Jones, J.A. Implementation of energy harvesting system for powering thermal gliders for long duration ocean research. In Proceedings of the OCEANS Conference, Washington, DC, USA, 19–22 October 2015.
- Blidberg, D.R. Solar-powered autonomous undersea vehicles. *Sea Technol.* **1997**, *38*, 45–52.
- Atmaram, G.; Ventre, G.G.; Maytrott, C.W.; Dunlop, J.P.; Swamy, R. Long term performance and reliability of crystalline silicon photovoltaic modules. In Proceedings of the 25th IEEE Photovoltaic Specialists Conference, Washington, DC, USA, 13–17 May 1996; pp. 1279–1282.
- Asaro, E.A. Solar Power for Autonomous Floats. *J. Atmos. Ocean. Technol.* **2007**, *24*, 1309–1314.
- Stahl, A. The utilization of the power of ocean waves. *Trans. Am. Soc. Mech. Eng.* **1892**, *13*, 438–506.
- McCormick, M.E. *Ocean Wave Energy Conversion*; Wiley: New York, NY, USA, 1981.
- Engineering Committee on Oceanic Resources Working Group on Wave Energy Conversion. *Wave Energy Conversion*; Elsevier Science Ltd.: Amsterdam, The Netherlands, 2003.
- Polinder, H.; Scuotto, M. Wave energy converters and their impact on power systems. In Proceedings of the International Conference on Future Power Systems, Amsterdam, The Netherlands, 18 November 2005; pp. 9–18.
- Previsic, M. Wave Power Technologies. *IEEE Power Eng. Soc. Gen. Meet.* **2005**, *2*, 2011–2016.
- Ringwood, J. The dynamics of wave energy. In Proceedings of the Irish Signals and Systems Conference (ISSC 2006), Dublin, Ireland, 28–30 June 2006.
- Penalba, M.; Ringwood, J. A Review of Wave-to-Wire Models for Wave Energy Converters. *Energies* **2016**, *9*, 506. [[CrossRef](#)]
- Li, L.; Yuan, Z.; Gao, Y. Maximization of energy absorption for a wave energy converter using the deep machine learning. *Energy* **2018**, *165*, 340–349. [[CrossRef](#)]
- Li, L.; Yuan, Z.; Gao, Y.; Zhang, X. Wave Force Prediction Effect on the Energy Absorption of a Wave Energy Converter with Real-Time Control. *IEEE Trans. Sustain. Energy* **2019**, *10*, 615–624. [[CrossRef](#)]
- Wang, L.; Isberg, J.; Tedeschi, E. Review of control strategies for wave energy conversion systems and their validation: The wave-to-wire approach. *Renew. Sustain. Energy Rev.* **2018**, *81*, 366–379. [[CrossRef](#)]
- Genest, R.; Davidson, J.; Ringwood, J.V. Adaptive control of a wave energy converter. *IEEE Trans. Sustain. Energy* **2018**. [[CrossRef](#)]
- António, F.D.O. Wave energy utilization: A review of the technologies. *Renew. Sustain. Energy Rev.* **2010**, *14*, 899–918.

26. Falcão, A.F.O.; Henriques, J. Oscillating-water-column wave energy converters and air turbines: A review. *Renew. Energy* **2016**, *85*, 1391–1424. [[CrossRef](#)]
27. Viviano, A.; Naty, S.; Foti, E.; Bruce, T.; Allsop, W.; Vicinanza, D. Large-scale experiments on the behaviour of generalised Oscillating Water Column under random waves. *Renew. Energy* **2016**, *99*, 875–887. [[CrossRef](#)]
28. Torre-Enciso, Y.; Ortubia, I.; De Aguilera, L.L.; Marqués, J. Mutriku wave power plant: From the thinking out to the reality. In Proceedings of the 8th European Wave Tidal Energy Conference, Uppsala, Sweden, 10 September 2009; pp. 319–329.
29. Dorrell, D.G.; Halliday, J.R.; Miller, P.; Findlater, M. Review of wave energy resource and oscillating water column modelling. In Proceedings of the 39th International Universities Power Engineering Conference, Bristol, UK, 6–8 September 2004; Volume 1, pp. 649–653.
30. Kofoed, J.P.; Frigaard, P.; Friis-Madsen, E.; Sørensen, H.C. Prototype testing of the wave energy converter wave dragon. *Renew. Energy* **2006**, *31*, 181–189. [[CrossRef](#)]
31. Vicinanza, D.; Nørgaard, J.H.; Contestabile, P.; Andersen, T.L. Wave loadings acting on overtopping breakwater for energy conversion. *J. Coast. Res.* **2013**, *2*, 1669–1674. [[CrossRef](#)]
32. Sabzehgar, R.; Moallem, M. A review of ocean wave energy conversion systems. In Proceedings of the Electrical Power & Energy Conference (EPEC), Montreal, QC, Canada, 22–23 October 2009.
33. Wu, F.; Zhang, X.P.; Ju, P.; Sterling, M.J.H. Modeling and control of AWS-based wave energy conversion system integrated into power grid. *IEEE Trans. Power Syst.* **2008**, *23*, 1196–1204.
34. Polinder, H.; Mecrow, B.C.; Jack, A.G.; Dickinson, P.G.; Mueller, M.A. Conventional and TFPM linear generators for direct-drive wave energy conversion. *IEEE Trans. Energy Convers.* **2005**, *20*, 260–267. [[CrossRef](#)]
35. Kim, J.S.; Kim, J.Y.; Park, J.B. Estimation of incident wave of AWS-based wave energy converter using extended Kalman filter. In Proceedings of the International Conference on Control and Automation, Gwangju, Korea, 20–23 October 2013; pp. 1411–1416.
36. Yemm, R.; Pizer, D.; Retzler, C.; Henderson, R. Pelamis: Experience from concept to connection. *Philos. Trans. R. Soc. A* **2012**, *370*, 365–380. [[CrossRef](#)]
37. Sjökvist, L.; Krishna, R.; Rahm, M.; Castellucci, V.; Anders, H.; Leijon, M. On the Optimization of Point Absorber Buoys. *J. Mar. Sci. Eng.* **2014**, *2*, 477–492. [[CrossRef](#)]
38. Falnes, J.; Hals, J. Heaving buoys, point absorbers and arrays. *Philos. Trans. R. Soc. A* **2012**, *370*, 246–277. [[CrossRef](#)] [[PubMed](#)]
39. Faizal, M.; Ahmed, M.R.; Lee, Y. A Design Outline for Floating Point Absorber Wave Energy Converters. *Adv. Mech. Eng.* **2014**, *6*, 846097. [[CrossRef](#)]
40. Henriques, J.C.C.; Portillo, J.C.C.; Gato, L.M.C.; Gomes, R.P.F.; Ferreira, D.N.; Falcão, A.F.O. Design of oscillating-water-column wave energy converters with an application to self-powered sensor buoys. *Energy* **2016**, *112*, 852–867. [[CrossRef](#)]
41. Budar, K.; Falnes, J. A resonant point absorber of ocean-wave power. *Nature* **1975**, *256*, 478. [[CrossRef](#)]
42. Wang, L.; Engström, J.; Götteman, M.; Isberg, J. Constrained optimal control of a point absorber wave energy converter with linear generator. *J. Renew. Sustain. Energy* **2015**, *216*, 415–423. [[CrossRef](#)]
43. Naeije, M.; Scharroo, R.; Doornbos, E. The Next Generation Altimeter Service Challenges and Achievements. In Proceedings of the Envisat Symposium 2007, Montreux, Switzerland, 23–27 April 2007.
44. Chongfei, S.; Zhirong, L.; Jianzhong, S.; Zhongyue, L.; Yiming, Z.; Guoheng, W. Design and Numerical Analysis of a Novel Counter-Rotating Self-Adaptable Wave Energy Converter Based on CFD Technology. *Energies* **2018**, *11*, 694.
45. Bascom, W. *Waves and Beaches*; Doubleday: New York, NY, USA, 1964.
46. Phillips, O.M. *The Dynamics of the Upper Ocean*, 2nd ed.; Cambridge University Press: Cambridge, UK, 1977; ISBN 0-521-29801-6.
47. Goda, Y. *Random Seas and Design of Maritime Structures*; World Scientific: Singapore, 2000; ISBN 978-981-02-3256-6.
48. Whitham, G.B. *Linear and Nonlinear Waves*; Wiley: New York, NY, USA, 1974; pp. 11–12.
49. Williams, C.B.; Yates, R.B. Analysis of a micro-electric generator for microsystems. *Sens. Actuator A* **1996**, *52*, 8–11. [[CrossRef](#)]
50. Polnikov, V.G.; Lavrenov, I.V. Calculation of the Nonlinear Energy Transfer through the Wave Spectrum at the Sea Surface Covered with Broken Ice. *Oceanology* **2007**, *47*, 334–343, ISSN 0001-4370. [[CrossRef](#)]

51. Pierson Moskowitz-Defines the Pierson Moskowitz Spectra in the Wave-Frequency Domain. Available online: http://www.codecogs.com/library/engineering/fluid_mechanics/waves/spectra/pierson_moskowiz.php (accessed on 6 June 2018).
52. Surface Velocity Program (SVP) Drifter. Available online: http://gdp.ucsd.edu/ldl_drifter/instruments/svp.html (accessed on 22 June 2018).



© 2019 by the authors. Licensee MDPI, Basel, Switzerland. This article is an open access article distributed under the terms and conditions of the Creative Commons Attribution (CC BY) license (<http://creativecommons.org/licenses/by/4.0/>).